European Journal of Pharmaceutical Sciences 180 (2023) 106336

Contents lists available at ScienceDirect

European Journal of Pharmaceutical Sciences

journal homepage: www.elsevier.com/locate/ejps

Biological evaluation of integrin $\alpha_3\beta_1$-targeted ^{68}Ga-labeled HEVNPs in HCT 116 colorectal tumor-bearing mice

Elisavet Lambidis [a], Chun-Chieh Chen [b], Dave Lumen [a], Ana Isabel Fraguas Sánchez [a], Mirkka Sarparanta [a], R. Holland Cheng [b,*], Anu J. Airaksinen [a,c,*]

[a] Department of Chemistry, Radiochemistry, University of Helsinki, Helsinki FI-00014, Finland
[b] Department of Molecular and Cellular Biology, University of California, Davis, CA 95616, U.S.A.
[c] Turku PET Centre, Department of Chemistry, University of Turku, Turku FI-20520, Finland

ARTICLE INFO

Keywords:
Gallium-68
DOTA
Virus-like particle
Hepatitis E viral nanoparticles
LXY30
HCT 116 colorectal cancer cells

ABSTRACT

Integrins are cell surface receptors involved in multiple functions vital for cellular proliferation. Various tumor cells overexpress αβ-integrins, making them ideal biomarkers for diagnostic imaging and tumor-targeted drug delivery. LXY30 is a peptide that can specifically recognize and interact with the integrin $\alpha_3\beta_1$, a molecule overexpressed in breast, ovarian and colorectal cancer. Hepatitis E virus nanoparticles (HEVNPs) are virus-like particles that have been investigated as drug delivery agents for the targeted delivery of nucleic acids and small proteins. HEVNPs can be a theranostic platform for monitoring and evaluating tumor-targeted therapies if tagged with a suitable diagnostic marker. Herein, we describe the radiolabeling and biological evaluation of integrin $\alpha_3\beta_1$-targeted HEVNPs. HEVNPs were conjugated with DOTA and radiolabeled with gallium-68 ($t_{1/2}$ = 67.7 min), a short-lived positron emitter used in positron emission tomography (PET). The synthesized [^{68}Ga]Ga-DOTA-HEVNPs were used to evaluate the efficacy of conjugated LXY30 peptide to improve HEVNPs binding and internalization to integrin $\alpha_3\beta_1$ expressing human colorectal HCT 116 cells. *In vivo* tumor accumulation of [^{68}Ga]Ga-DOTA-HEVNP-LXY30 was evaluated in HCT 116 colorectal tumor-bearing mice. [^{68}Ga]Ga-DOTA-HEVNP-LXY30 and non-targeted [^{68}Ga]Ga-DOTA-HEVNP were radiolabeled with radiochemical yields (RCY) of 67.9 ± 3.3% and 73.7 ± 9.8%, respectively. [^{68}Ga]Ga-DOTA-HEVNP-LXY30 exhibited significantly higher internalization in HCT 116 cells than the non-targeted [^{68}Ga]Ga-DOTA-HEVNPs (21.0 ± 0.7% vs. 10.5 ± 0.3% at 3 h, $^{****}P<0.0001$). After intravenous administration to mice, accumulation of [^{68}Ga]Ga-DOTA-HEVNP-LXY30 to HCT 116 xenograft tumors was at its highest rate of 0.8 ± 0.4%ID/g at 60 min. [^{68}Ga]Ga-DOTA-HEVNP-LXY30 accumulated mainly in the liver and spleen (39.8 ± 13.0%%ID/g and 24.6 ± 24.1%ID/g, respectively). Despite the low targeting efficiency *in vivo*, we demonstrated that [^{68}Ga]Ga-DOTA-HEVNP is a promising diagnostic platform for quantitative analysis of HEVNP distribution *in vivo*. This nanosystem can be utilized in future studies assessing the success of further engineered HEVNP structures with optimized targeting efficiency *in vivo*.

1. Introduction

Colorectal cancer is the third most frequent cancer type worldwide after lung and breast malignancies (Parkin et al., 2005, Labianca et al., 2010, Kim et al., 2017, Ludvigsen et al., 2020). Countries of the West and North are mainly affected, with higher incidence rates in the industrialized and high-income countries. For instance, 9% of newly diagnosed malignancies emanated from the colon in Europe (Parkin et al., 2005, Labianca et al., 2010, Kim et al., 2017). Colorectal carcinoma has the second-highest mortality, because many patients suffer from metastases that are challenging to treat (Wang et al., 2021). Therefore, it is important to develop methods to provide early and accurate diagnosis and treatment.

Colorectal cancer is typically diagnosed by colonoscopy and biopsies. Currently, in order to complement the moderate sensitivity of the conventional colonoscopy, molecular imaging, such as positron emission tomography (PET), is increasingly used in colorectal tumor diagnosis, offering higher sensitivity and detecting possible metastatic lesions. Furthermore, fluorescent or near-infrared fluorescent-labeled antibodies and small molecules like peptides and enzymes have been

* Corresponding authors.
E-mail addresses: rhch@ucdavis.edu (R.H. Cheng), anu.airaksinen@utu.fi (A.J. Airaksinen).

https://doi.org/10.1016/j.ejps.2022.106336
Received 11 August 2022; Received in revised form 10 November 2022; Accepted 16 November 2022
Available online 17 November 2022

developed for intra-operative optical imaging of colorectal lesions (Kim et al., 2017, Kashihara et al., 2021, Goetz and Wang, 2010). Although surgical resection combined with chemotherapy and radiotherapy is the most widely used therapy for colorectal carcinoma, in the case of metastasis, the tumors may not be easily surgically removable. Thus, there is a need for alternative and complementary therapies. Targeted therapies are new emerging therapies for colorectal cancer, and new antibody-based therapies have improved survival for colorectal cancer patients (Xie, Chen, and Fang, 2020). Nanoparticle (NP)-based therapies are increasingly investigated as drug carriers for targeted therapy for colorectal cancer (Wahab et al., 2021). When combined with a diagnostic function, they can be used as nanotheranostics allowing monitoring of the targeting efficacy during the therapy. Currently, there are no clinically approved nanomedicines for colorectal cancer, but several are in clinical trials (He et al., 2019).

Hepatitis E virus nanoparticles (HEVNPs) are promising protein-based nanomaterials for targeted drug delivery and diagnostics. They are derived from the corresponding virus without the genetic material. Without a capability to replicate, HEVNPs are safe (non-toxic and biocompatible), small (20-30 nm in diameter), and due to their protein structure, they are also biodegradable (into amino acids). In addition, the primary immunogenic region of HEVNP is positioned on the apex of the protruding arms, pointing away from the capsid shell. Consequently, modifications to these protruding arms have been shown to eliminate (or significantly reduce) humoral immune detection, making the HEVNP system amenable to repeated dosing. The icosahedral capsid of the HEVNP is composed of sixty copies of three-domain (S: shell, M: middle, and P: protrusion domain) subunits responsible for the highly ordered configuration and, thus, high stability of the capsid NPs. Moreover, the HEVNPs can self-assemble and self-disassemble depending on the environment. Consequently, payloads can be encapsulated into HEVNPs, enabling their use in theranostic applications. HEVNPs can harbor diverse payloads, such as nucleic acids or therapeutics, including insulin (Takamura et al., 2004, Jariyapong et al., 2013, Baikoghli et al., 2018, Panda et al., 2015, Ganganboina et al., 2021). The tight capsid protects the drug from early release while enhancing its permeability and retention, currently a significant limitation in cancer therapy (Senapati et al., 2018). The HEVNP surface can also be efficiently functionalized, introducing ligands, peptides, or contrast agents to the NP exterior. The above characteristics of HEVNPs give rise to their utilization as multi-modal imaging agents (Baikoghli et al., 2018, Chen et al., 2016, Xing et al., 1999, Cheng, 2018).

Furthermore, the non-invasive and functional imaging modality PET offers the highest sensitivity with respect to the other molecular imaging techniques, such as optical, magnetic resonance imaging, ultrasound, and single-photon emission computed tomography (SPECT). Previously we reported that HEVNPs could be efficiently radiolabeled with a PET radionuclide ($^{68}Ga^{3+}$) using a DOTA chelator, resulting in a highly stable radiolabeled NP system under both *in vitro* and *in vivo* conditions (Lambidis et al., 2022).

The αβ heterodimeric transmembrane glycoproteins are integrins in the extracellular matrix and basement membranes (Xiao et al., 2019, Carney et al., 2017). These cell surface receptors are involved in the intracellular signaling between extracellular matrix substrates and the cell cytoplasm by interacting with signaling molecules (Dydensborg et al., 2009). Mainly due to the β subunit (Xiao et al., 2019), integrins are involved in numerous stages of several biological processes that induce cellular proliferation, such as cell adhesion, inflammation, angiogenesis, signal-transduction and metastasis, while they preventing cell apoptosis. Usually, specific arrangements of integrins are overexpressed on activated endothelial cells and in specific cancerous cells and result in distinct biological functions (Xiao et al., 2019, Carney et al., 2017, Chen et al., 2004). Therefore, integrins can serve as valuable biomarkers for targeted imaging and treatment of selected cancer types (Xiao et al., 2019, Chen et al., 2004, Xiao et al., 2016). For example, the β_1 subunit is associated with the malignant phenotype in breast tumors and the metastasis in specific cancers, including ovarian and lung cancer (Pelillo et al., 2015). The β_1 chain can form a heterodimer with the α_3 subunit. The integrin $\alpha_3\beta_1$ is expressed in normal tissues, including the liver, lung, kidney and muscle, and is needed for the tissue growth.

Additionally, the integrin is overexpressed in multiple human cancer cells in which it promotes the migration of cancer cells. Examples of these cancers are glioblastoma, ovarian, breast, lung, and colon cancer (Xiao et al., 2016, Sloan et al., 2006, Chin et al., 2019). The α_3 subunit is recognized and bound by the LXY30 cyclic peptide ligand (Xiao et al., 2016). Due to the specific binding of the α_3 subunit to the β_1 subunit, LXY30 has been characterized as ideal for targeting specifically the integrin $\alpha_3\beta_1$ (Carney et al., 2017, Xiao et al., 2016). The highly potent LXY30 peptide ligand has shown a robust binding affinity toward the integrin $\alpha_3\beta_1$ expressed on glioblastoma cells (Xiao et al., 2016), non-small-cell lung carcinoma, breast (Xiao et al., 2019, Carney et al., 2017), ovarian, and brain cancer cells. The sequence specificity of LXY30 has also been proven (Carney et al., 2017).

The human colorectal carcinoma cell line, HCT 116 (ATCC CCL-247™), is an example of a cell line for which the cell membrane expression of various α and β subunits as well as of complete heterodimeric integrins has been evaluated *in vitro*. The integrin expression profile revealed that the level and/or activity of the integrins present on the cell membrane of the HCT 116 cells influences and is directly proportional to the adhesion potential of the HCT 116 cells to the extracellular matrix proteins, and thus to the tumor development (Pelillo et al., 2015). For instance, the overexpression of the extracellular epitopes of the human α_3 chain together with the β_1 chain (Pelillo et al., 2015, Ahmed et al., 2003), depicted the desired adhesion of the HCT 116 cells to laminin. The integrin $\alpha_3\beta_1$ is one of the main integrins on the HCT 116 cancer cells that mediate the cell interactions with extracellular matrix substrates that are vital for the progression of the disease (Pelillo et al., 2015). This study aimed to develop a radiolabeled HEVNP-LXY30 system and evaluate its targeting capability toward HCT 116 colorectal cancer cells and murine 4T1 breast cancer cells *in vitro*, and in an HCT 116 tumor-bearing mouse model.

2. Materials and methods

All chemicals and solvents were obtained from commercial providers and used without further purification. HEVNPs (in 10 mM MES (2-(N-morpholino)ethanesulfonic acid) buffer, pH 6.2, >10 mg/ml) and the targeted HEVNPs, HEVNP-LXY30 (peptide sequence: cdG-Phe(3,5-diF)-G-Hyp-NcR (Xiao et al., 2016)) (in 10 mM MES pH 6.2 buffer, >20 mg/ml), were prepared as previously described (Chen et al., 2016). DOTA-NHS ester (1,4,7,10-tetraazacyclododecane-1,4,7,10-tetraacetic acid mono-N-hydroxysuccinimide ester) was purchased from Macrocyclics (Plano, TX, U.S.A.). All the water was ultra-pure (>18.2 $M\Omega cm^{-1}$) and was prepared on a Milli-Q Integral 10 water purification system. For each buffer preparation, the ultra-pure water was treated with Chelex 100 sodium form (Sigma-Aldrich, St. Louis, MO, U.S.A.) at a 5 g/l to eliminate trace metals. The PD-10 Sephadex G-25 M desalting columns were obtained from GE Healthcare (Chicago, IL, U.S.A.) and preconditioned prior to use with 20 ml phosphate buffer saline (PBS; 0.01 M, pH 7.4). The human plasma was obtained from Finnish Red Cross (Helsinki, Finland, license no. 33/2018). HEVNP size and morphology were determined with TEM (JEOL1400, JEOL Ltd., Akishima, Tokyo, Japan). The protein concentration was measured using a μDrop Plate on a Multiskan Sky Microplate Spectrophotometer from Thermo Scientific (Waltham, MA, U.S.A.). For the ^{68}Ga-elution, the water TraceSELECT™ was acquired from Honeywell-Riedel-de Häen™ (Seelze, Germany), and the ultrapure 30% HCl (hydrochloric acid) was purchased from Merck (Kenilworth, NJ, U.S.A.). The ^{68}Ge/^{68}Ga generators (1.85 or 2.41 GBq at calibration) were GalliaPharm type generators produced by Eckert & Ziegler (Berlin, Germany). The radiochemical yield and purity were determined by Whatman 1 paper chromatography with 0.5 mM DTPA as the mobile phase. A photostimulated luminescence scanner FLA 5100

(Fujifilm, Tokyo, Japan) was used for the digital autoradiography using a Fuji TR323309 imaging plate and a 24 × 30 X-ray cassette. The automatic gamma counter was a 1480 Wizard® 3" (PerkinElmer™ Life Sciences, Waltham, MA, U.S.A.) and used with 60 s measurement time per sample. Cryosectioning was done on a Leica Biosystems (Germany) CM1950 cryostat microtome. The Optimal Cutting Temperature (O.C.T.) mounting medium and the SuperFrost® Plus microscope slides were purchased from VWR® (Radnor, PA, U.S.A.). The sections were scanned with a real-time digital autoradiography BeaQuant™ system from AI4R (Nantes, France). The HCT 116 human colorectal carcinoma (CCL-247™) and murine 4T1 breast cancer (CRL-2539™) cell lines were purchased from ATCC® (Manassas, VA, U.S.A.). More information on cell culture conditions can be found in the Supplementary Information (SI).

2.1. Functionalization of HEVNP-LXY30 with DOTA for radiolabeling

Buffer exchange was done for the targeted HEVNP-LXY30 stock (5.3 mg/ml) in 10 mM MES pH 6.2 using a preconditioned PD-10 column and 0.01 M phosphate buffer (PB) (pH 7.4) elution buffer. HEVNP-LXY30 (1.5 mg, were diluted in 0.01 M PB (pH 7.4)) into a final volume of 250 μl (1.1 mg/ml or 19.7 μM, 28.1 nmol). DOTA-NHS ester (21.3 mg, 33.7 μmol) was dissolved in 0.01 M PB (pH 7.4) to a final concentration of 23.54 mM and a final volume of 250 μl. The NHS ester solution was added *dropwise* to the reaction tube (1.5-ml Protein LoBind microtube, Eppendorf) containing the HEVNP-LXY30. The mixture was immediately mixed well by careful pipetting. Sodium hydrogen carbonate (0.1 M, pH 9) was used for adjusting the pH to 7.3. The final reaction volume was 1430 μl. The reaction mixture was shaken (400 rpm) at RT for 4 h, and then at 4°C overnight. Two preconditioned PD-10 columns were used consecutively for the complete purification of the conjugated NPs by gravity size exclusion chromatography (SEC). The last elution of the NPs was done with 2.5 ml of 0.01 M PBS (pH 7.4).

2.2. Functionalization of HEVNP with DOTA for radiolabeling

HEVNPs (1 mg, 23.34 mg/ml, 10 mM MES pH 6.2) were diluted in 0.01 M PB (pH 7.4) into a final volume of 250 μl (2 mg/ml or 37.6 μM, 18.8 nmol). DOTA-NHS ester (18 mg, 23.6 μmol) was dissolved in 0.01 M PB (pH 7.4) to a final concentration of 45 mM and a final volume of 250 μl. The NHS ester solution was added *dropwise* to the reaction tube (1.5-ml Protein LoBind microtube, Eppendorf) containing the NPs. The mixture was immediately mixed well by careful pipetting. Sodium hydrogen carbonate (0.1 M, pH 9) was used for adjusting pH to 7.4. The final reaction volume was 1100 μl. The reaction mixture was shaken (500 rpm) at RT for 3 h, and then at 4°C overnight. A PD-10 column was used to purify the conjugated NPs by gravity SEC (size exclusion chromatography) by eluting the conjugated NPs with 3 ml of 0.01 M PBS (pH 7.4).

2.3. Radiolabeling and purification of the DOTA-functionalized HEVNP-LXY30

DOTA-HEVNP-LXY30 (0.21 mg/ml in 200 μl in PB) were diluted with metal-free 0.25 M ammonium acetate buffer pH 7 (0.8 ml) in a reaction tube (5-ml Protein LoBind microtube, Eppendorf). This was followed by adding freshly eluted [^{68}Ga]$GaCl_3$ in 0.1 M HCl (80-140 MBq in 1 ml). The final reaction volume was 2 ml, and the reaction pH was 4.5. The reaction solution was mixed for 30 min at 63°C with 400 rpm. After 30 min, the reaction solution was cooled down to RT and immediately purified using a preconditioned PD-10 column. [^{68}Ga]Ga-DOTA-HEVNP-LXY30 were eluted with 1.8 ml of 0.01 M PBS (pH 7.4). The radiochemical yield and purity (following the PD-10 purification) of [^{68}Ga]Ga-DOTA-HEVNP-LXY30 were obtained by radio-TLC and were 67.9 ± 3.3% (RCY, n = 3) and 98.4 ± 0.4% (RCP, n = 3), respectively.

2.4. Radiolabeling and purification of the [^{68}Ga]Ga-DOTA-HEVNP control

HEVNPs (0.13 mg/ml in 100 μl in PB) were diluted with metal-free 0.25 M ammonium acetate buffer (0.8 ml) in a reaction tube (5-ml Protein LoBind microtube, Eppendorf). This was followed by adding freshly eluted [^{68}Ga]$GaCl_3$ in 0.1 M HCl (80–140 MBq in 1 ml). The final reaction volume was 1.9 ml, and the reaction pH was 4.5. The reaction solution was mixed for 30 min at 63°C with 350 rpm. The reaction solution was then cooled down to RT, and the mixture was immediately purified using a preconditioned PD-10 column. [^{68}Ga]Ga-DOTA-HEVNP were eluted with sterile 0.01 M PBS (pH 7.4). The radiochemical yield and purity (following the PD-10 purification) of [^{68}Ga]Ga-DOTA-HEVNP were estimated by radio-TLC and were 73.7 ± 9.8% (RCY, n = 3) and 98.5 ± 0.3% (RCP, n = 3), respectively.

2.5. In vitro stability of [^{68}Ga]Ga-DOTA-HEVNP-LXY30

[^{68}Ga]Ga-DOTA-HEVNP-LXY30 (700 μl in PB; 1.8-2.2 MBq) were added into 1.5-ml Protein LoBind microtubes containing 700 μl of PBS (0.01 M, pH 7.4), 100% human plasma, iron ($FeCl_3 \cdot 6\ H_2O$, 18 mM in PBS), or CO_2-independent cell medium (from Gibco). All the samples (n = 3 per testing solution) were incubated at 37°C. The amount of the intact ^{68}Ga-radiolabeled HEVNP-LXY30 was monitored by radio-TLC at 5 min, 15 min, 30 min, and 60 min after the initiation of the incubation with the testing solutions.

2.6. Cell uptake study of the targeted [^{68}Ga]Ga-DOTA-HEVNP-LXY30, [^{68}Ga]Ga-DOTA-HEVNP, and [^{68}Ga]$GaCl_3$ controls

The day before the study, the human HCT 116 colorectal or murine 4T1 breast cancer cells were plated in the CO_2-independent medium on sterile 12-well plates (2.2 million HCT 116 or 4T1 cells/ml/well). The following day, the medium was removed 2 hr prior to the initiation of the study, and the cells were incubated at 37°C with either the targeted [^{68}Ga]Ga-DOTA-HEVNP-LXY30, the non-targeted [^{68}Ga]Ga-DOTA-HEVNP or the free ^{68}Ga-radionuclide. Both types of NPs and the free radionuclide were diluted in fresh CO_2-independent medium prior their addition into the cells until the radioactivity was the same for all the cases per well (0.2 MBq/well). The incubation time varied depending on the time point (15, 30, 60, 120 and 180 min). The detailed cell uptake procedure is given in SI.

2.7. Ex vivo biodistribution of [^{68}Ga]Ga-DOTA-HEVNP-LXY30 and [^{68}Ga]Ga-DOTA-HEVNP control

All animal experiments were carried out under a project license approved by the National Board of Animal Experimentation in Finland (ESAVI/12132/04.10.07/2017) and in compliance with the respective institutional, national, and EU regulations and guidelines. The mice were group-housed in standard polycarbonate cages with aspen bedding, nesting material (Tapvei, Harjumaa, Estonia), and enrichment (aspen blocks and disposable cardboard hut). Pelleted food (Teklad 2019C diet, Envigo, Horst, Netherlands) and tap water were available *ad libitum*. Environmental conditions of a 12:12 light/dark cycle, the temperature of 22 ± 1°C, and relative humidity of 55 ± 15% were maintained throughout the study.

The *ex vivo* biodistribution was studied in 13 HCT 116 colorectal tumor-bearing female nude Naval Medical Research Institute (NMRI) mice (Janvier, 7-8 weeks, 17-20 g, n = 4 per time point). For the control experiment, the *ex vivo* biodistribution was done in 3 tumor-bearing female nude NMRI mice (Janvier, 7-8 weeks, 17-20 g, n = 1 per time point). For the HCT 116 tumor-bearing mice, 2 × 10^6 HCT 116 cells in 100 μl of sterile 1 × HBSS were introduced to each mouse subcutaneously under 2.5% isoflurane anesthesia in medical air:oxygen (3:2) carrier. The tumors were allowed to grow for 20-23 days prior to the

administration of the radiolabeled NPs, reaching 7.9-8.9 mm in diameter.

The [^{68}Ga]Ga-DOTA-HEVNP-LXY30 (0.023 ± 0.0050 mg/ml, 0.2–0.5 MBq) or [^{68}Ga]Ga-DOTA-HEVNP (control; 0.14 ± 0.031 mg/ml, 0.2–0.5 MBq) nanoparticles were injected into the tail vein in 200 μl of PB pH = 7.4. The mice were sacrificed with CO_2 asphyxiation at 15 min, 30 min and 60 min after the injection, and selected organs were harvested. The harvested organs were weighed and counted by a gamma counter, and the radioactivity decay was corrected at the start of the measurement. Standards were prepared using 10 μl of the formulated [^{68}Ga]Ga-DOTA-HEVNPs suspension and measured before the tissues. The results are expressed as the percent injected dose per gram of tissue (%ID/g).

2.8. Autoradiography of [^{68}Ga]Ga-DOTA-HEVNP-LXY30 and [^{68}Ga]Ga-DOTA-HEVNP control in HCT 116 colorectal xenograft tumor

One HCT 116 colorectal xenograft tumor from each time point and one liver from the 1 h time point was collected for autoradiography followed the *ex vivo* biodistribution study. Cold isopentane and dry ice were used to snap-freeze the tumors. These were then embedded in O.C.T. tissue-freezing medium and consequently sectioned with a cryostat microtome. The section thickness was 10 μm, and the sections were collected on SuperFrost Plus microscope slides. The sections were scanned for 16-17 h on a real-time BeaQuant autoradiographic device.

2.9. Statistical analysis

The average values of the quantitative data between groups were analyzed for statistical significance using an unpaired two-tailed *t*-test on GraphPad Prism 9 (San Diego, CA, USA), with a *P* value equal or less than 0.05 considered statistically significant (*$P \leq 0.05$, **$P \leq 0.01$, ***$P \leq 0.001$, ****$P \leq 0.0001$ and ns (non-significant) when $P > 0.05$).

3. Results and discussion

HEVNPs consist of three surface variable loops on the P domain. These, together with the C terminal of the HEV capsid protein (open reading frame 2, ORF2), enable various chemical conjugations to the HEVNP surface (Rohovie, Nagasawa, and Swartz, 2017). The surface loops can be designed and engineered as conjugation sites for at least one molecule, such as a bioactive agent (Baikoghli et al., 2018, Chen et al., 2016, Smith, Hawes, and Bundy, 2013). The latter is then well-exposed on the HEVNP surface without compromising the native icosahedral structure. For instance, the P domain contains 60 cysteine amino acids. Cysteines reduce the responses of pre-existing antibodies to HEVNPs, which is the major shortcoming of a protein-based delivery vector. In addition, cysteines can be used as chemical conjugation sites. In other words, the surface engineering of HEVNPs is allowed by replacing cysteines with desired molecules or functional groups. Furthermore, with 60 identical and repeated units of capsid proteins, a single site-specific modification results in 60 symmetric sites for the chemical modulation of multiple foreign molecules. Due to these 60 units (ORF2), the highly ordered HEVNP system remains stable under the conjugation conditions as well as the storage and physiological conditions (Jariyapong et al., 2013, Xing et al., 1999, Smith, Hawes, and Bundy, 2013, Koudelka and Manchester, 2010, Zafrullah et al., 2004). In this study, an HEVNP surface modification to yield targeted HEVNPs bearing the LXY30 targeting ligand peptide was done (Jariyapong et al., 2013, Baikoghli et al., 2018, Chen et al., 2016, G Kamita et al., 2020). For this conjugation, the cysteine conjugation sites of the P domain were occupied. Therefore, further desired surface modifications had to be driven toward other conjugation sites. Apart from cysteines, HEVNPs contain 60 lysine amino acids. Lysine contains a primary amine accessible for activated carboxylic acid esters, forming an amide bond. Here, the functionalization of the lysines with a DOTA-NHS ester allowed the radiolabeling of the targeted HEVNPs with gallium-68. Non-targeted HEVNPs modified with DOTA in a similar strategy were used as controls. The successful coordination of the DOTA chelator with the gallium-68 radiometal requires elevated temperatures. Thus, initially, thermal stability experiments were performed to confirm the robustness of the HEVNP capsid relatively to different temperatures. The melting curve was measured via differential scanning fluorimetry (DSF) using qPCR. The results showed that HEVNPs were stable in phosphate buffer at pH 4.5 when temperature was kept below 80°C. The RCYs of the targeted [^{68}Ga]Ga-DOTA-HEVNP-LXY30 (67.9%, n = 3) and non-targeted [^{68}Ga]Ga-DOTA-HEVNP (73.7%, n = 3) HEVNPs were comparable, and thus the radiolabeling was proved not to be interfered by the peptide conjugation. The purification of the radiolabeled HEVNPs in both cases was done with a preconditioned PD-10 SEC column, and the obtained RCP was 98.4 ± 0.4% (RCP, n = 3) and 98.5 ± 0.3% (RCP, n = 3) for [^{68}Ga]Ga-DOTA-HEVNP-LXY30 and [^{68}Ga]Ga-DOTA-HEVNP, respectively.

The *in vitro* radiolabel stability of [^{68}Ga]Ga-DOTA-HEVNP-LXY30 was evaluated in 0.01 M PBS (pH 7.4), 50% human plasma, or cell medium at 37°C. The iron challenge was also performed to account for the high amount of iron found *in vivo,* which might result in the transchelation between $^{68}Ga^{3+}$ and Fe^{3+} cations. To investigate the competition, a high concentration of iron(III) was used (18 mM) as an excess of the normal iron levels in the blood (maximum physiological amount in blood for males: 32 μM (Pagana, Pagana, and Pagana, 2015)). The results (Fig.1) revealed high *in vitro* radiolabel stability of [^{68}Ga]Ga-DOTA-HEVNP-LXY30 under all tested conditions. In most cases, the amount of the intact radiolabeled NPs was at least 95%. Only after 60 min in plasma, some detachment of gallium-68 was observed (88.5 ± 0.1% intact tracer).

The cell uptake of [^{68}Ga]Ga-DOTA-HEVNP-LXY30 was studied in murine 4T1 breast and human HCT 116 colorectal cancer cells, which both have been reported to express integrin $\alpha_3\beta_1$ (Fig.2A) (Chin et al., 2019, Sloan et al., 2006). The [^{68}Ga]Ga-DOTA-HEVNP-LXY30 internalization in 4T1 cells remained low and was at maximum 1.6 ± 0.1% at 1 h. Additionally, [^{68}Ga]Ga-DOTA-HEVNP-LXY30 were not detected on the cell membrane of the 4T1 cells either (maximum membrane-bound

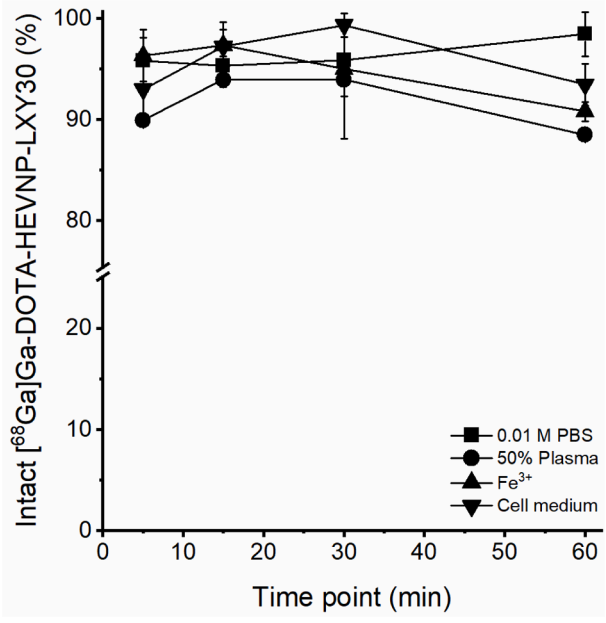

Fig. 1. In *vitro* stability of [^{68}Ga]Ga-DOTA-HEVNP-LXY30 at 37°C under constant shaking at 400 rpm in PBS (0.01 M, pH 7.4), 50% human plasma, $FeCl_3$ (0.2 mM) and CO_2-independent cell medium. The amount of intact [^{68}Ga]Ga-DOTA-HEVNP-LXY30 was estimated by radio-TLCs within the first hour of incubation. The values represent the average ± standard deviation (n = 2–3).

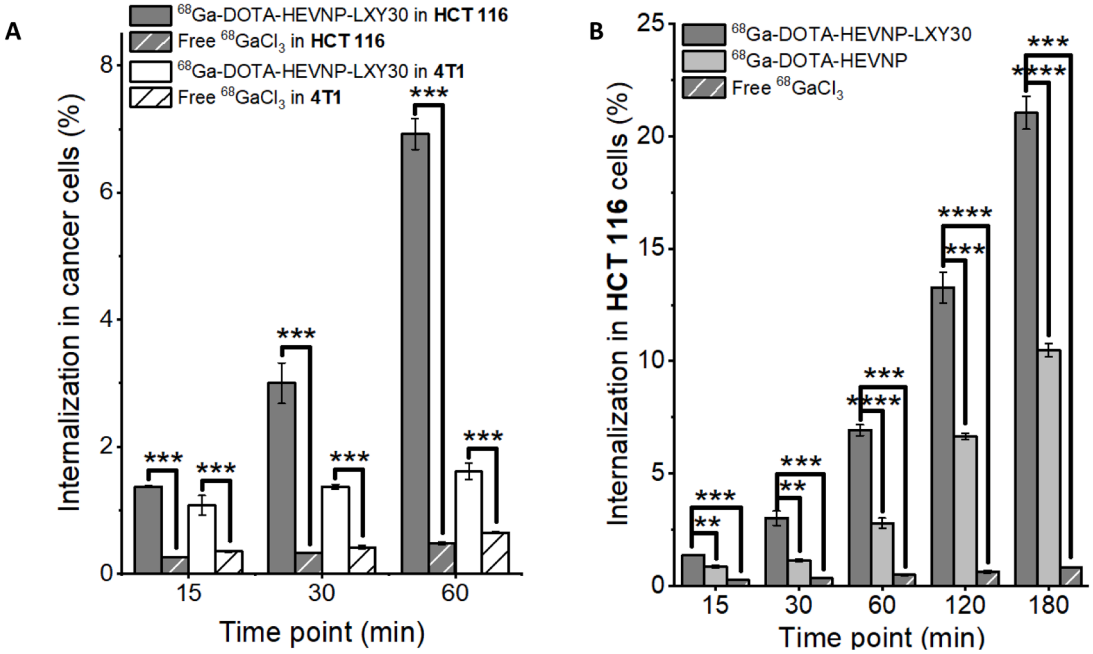

Fig. 2. Cell internalization of: (A) [^{68}Ga]Ga-DOTA-HEVNP-LXY30 and free [^{68}Ga]GaCl$_3$ in 4T1 breast and HCT 116 colorectal cancer cells, and (B) [^{68}Ga]Ga-DOTA-HEVNP-LXY30 (targeted HEVNPs), [^{68}Ga]Ga-DOTA-HEVNP (non-targeted HEVNPs) and free [^{68}Ga]GaCl$_3$ in HCT 116 colorectal cancer cells. The cell uptake assay was done at 37°C. The columns represent the average ± standard deviation (n = 3). Unpaired *t*-test was performed to assess the statistical significance of the difference between the two types of HEVNPs and between HEVNPs and free [^{68}Ga]GaCl$_3$((A): ***P=0.0003-0.001 and (B): ****P<0.0001).The membrane-bound fractions of the HEVNPs and radionuclide on the HCT 116 cells is shown in the SI (Fig.S1).

fraction 3.2% in 1 h). On the other hand, the cell uptake assay in HCT 116 colorectal cancer cells showed higher internalization of the targeted HEVNPs, [^{68}Ga]Ga-DOTA-HEVNP-LXY30. The internalization was gradually increased and was highly preferable, yielding 6.9 ± 0.2% of internalized NPs at 1 h and increasing to 21.0 ± 0.7% at 3h. Integrin $\alpha_3\beta_1$, is expressed in both cancer cell types, but the cells lines may have differences in their $\alpha_3\beta_1$ expression levels, which could explain the observed difference in 4T1 and HCT 116 internalization levels. Unfortunately, $\alpha_3\beta_1$-expression levels of the cells were not determined, preventing analysis of correlation between the integrin $\alpha_3\beta_1$-expression levels and the cell uptake. The high internalization of [^{68}Ga]Ga-DOTA-HEVNP-LXY30 in the HCT 116 cells was compared with the cell uptake assay of the controls, non-targeted [^{68}Ga]Ga-DOTA-HEVNP, and free [^{68}Ga]GaCl$_3$, that was completed in precisely the same way and simultaneously with the evaluation of [^{68}Ga]Ga-DOTA-HEVNP-LXY30 (Fig.2B). Some degree of cell internalization was revealed even for the non-targeted [^{68}Ga]Ga-DOTA-HEVNP. This is due to the internalization mechanism that HEV and HEVNPs follow, the clathrin-mediated endocytosis. This mechanism is responsible for the hepatotropism reported for HEV and HEVNPs (Lee et al., 2019, Kapur et al., 2012, Cao and Meng, 2012, Zheng et al., 2010, Lambidis et al., 2022). The clathrin-mediated endocytosis is typical also for several cancer cell lines, such as the HCT 116 colorectal cancer cells. It has been reported that HCT 116 allows the clathrin-mediated endocytosis of lysine-rich particles, thus contributing in increasing the uptake levels of HEVNPs (Horibe et al., 2018, Maraming et al., 2019). We have previously investigated this using our non-targeted HEVNP nanosystem because HEVNPs contain 60 lysine residues per particle, and thus can be considered lysine-rich (Lambidis et al., 2022). The amount of the internalized non-targeted NPs was half the amount of the targeted NPs at all time points. This profound difference between the two types of HEVNPs confirms the targeted capability of the NPs toward the HCT 116 colorectal cancer cell line. The membrane-bound fraction was equal to or less than 2.0% for both HEVNP types at all time points and equal to or less than 3.2% for [^{68}Ga]GaCl$_3$. Therefore, it could be concluded that the demonstrated interaction between the targeted HEVNPs and the HCT 116 cells was mainly due to the internalization of the NPs.

With the auspicious results from the cell uptake assay, the biodistribution of [^{68}Ga]Ga-DOTA-HEVNP-LXY30 was evaluated in mice bearing subcutaneous HCT 116 tumor xenografts after intravenous administration. The tumor uptake was less than 1%ID/g at all time points for both HEVNPs (Fig.3). On the other hand, in the case of the targeted NPs, an increase in tumor uptake was denoted. Starting from 0.5 ± 0.1%ID/g, the maximum detected activity due to [^{68}Ga]Ga-DOTA-HEVNP-LXY30 was 0.8 ± 0.4%ID/g after 1 h from the injection. Despite the increase, the uptake level was still low. However, PET imaging modality is such a powerful and sensitive technique that it might be possible to track the uptake of radiotracers as low as 1%ID/g. The highest levels of the [^{68}Ga]Ga-DOTA-HEVNP-LXY30 radioactivity were detected in the liver and the spleen. The highest uptake in the spleen was 32.0 ± 18.1%ID/g at only 15 min post-injection, and in the liver it was 39.8 ± 13.0%ID/g at 1 h, whereas for [^{68}Ga]Ga-DOTA-HEVNP only 5.4%ID/g was detected in the spleen at 15 min after the injection, and a maximum spleen uptake was detected at 30 min (8.4%ID/g). In addition, the liver uptake was higher in the case of [^{68}Ga]Ga-DOTA-HEVNP (above 51% at all time points) compared to [^{68}Ga]Ga-DOTA-HEVNP-LXY30.

Moreover, in the case of both HEVNP types, less than 3%ID/g was identified in all the tissues analyzed. An exception was the radioactivity level of [^{68}Ga]Ga-DOTA-HEVNP-LXY30 in the gallbladder which was less than 5.5%ID/g at all time points. This could be expected due to the variation in mouse metabolism. Additionally, even if HEVNP is larger than the molecular weight or size cut off of the glomerular filtration (6 nm in diameter size of NP (Xie et al., 2020)), the high radioactivity levels in urine could be due to HEVNP flexible nature (Wahab et al., 2021).

The low tumor uptake of [^{68}Ga]Ga-DOTA-HEVNP-LXY30 was probably due to the short circulation half-life and the HEVNPs' rapid sequestration into the liver. Consequently, as it can also be noted from Figure 4, both ratios with respect to the tumor, tumor-to-blood, and tumor-to-liver, were poor, with a maximum ratio of 0.45 (approximately 1:2 tumor:blood) at 1 h post-injection.

In addition, Figure 5 shows the blood and tumor time-activity curves

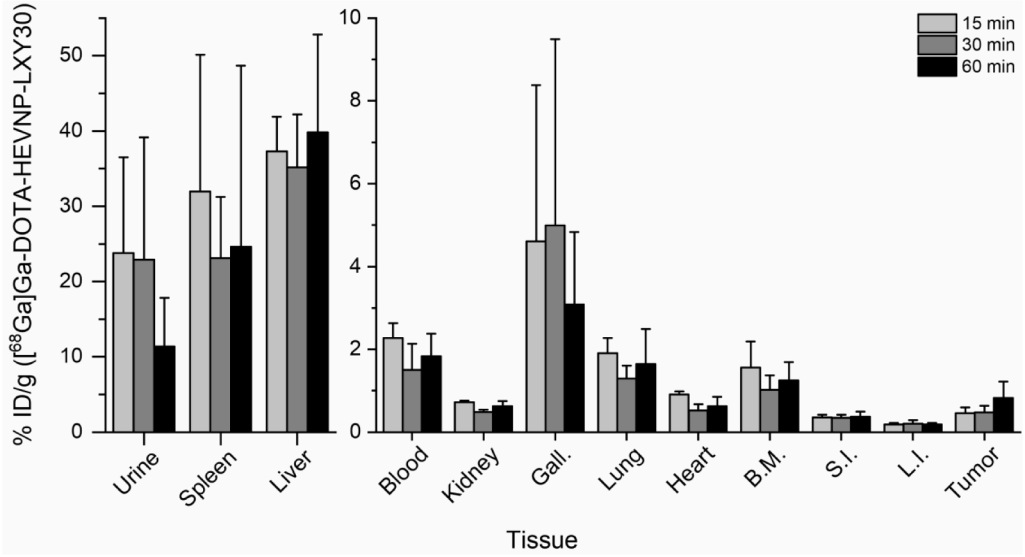

Fig. 3. *Ex vivo* biodistribution of [^{68}Ga]Ga-DOTA-HEVNP-LXY30 (n = 3-4) after the i.v. injection in HCT 116 colorectal tumor-bearing female nude NMRI mice obtained at 15, 30 and 60 min post-injection. The columns represent the average ± standard deviation. %ID/g = percent of injected dose per gram of tissue, Gall.: gallbladder, S.I.: small intestine, L.I.: large intestine, and B.M.: bone with marrow. The biodistribution of [^{68}Ga]Ga-DOTA-HEVNP-LXY30 was compared with the control ([^{68}Ga]Ga-DOTA-HEVNP), and the data can be found in the SI (Fig.S2).

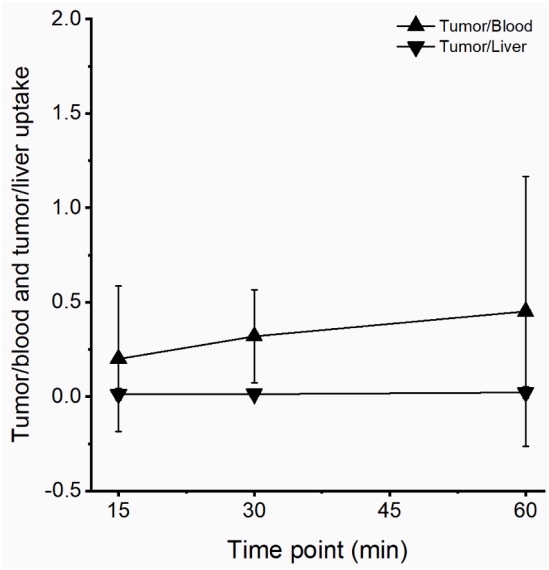

Fig. 4. Comparison of radioactivity levels of [^{68}Ga]Ga-DOTA-HEVNP-LXY30 in the tumor:blood and tumor:liver ratios against time following the *ex vivo* biodistribution in HCT 116 colorectal tumor-bearing female nude NMRI mice. The values represent the average ± standard deviation (n = 4).

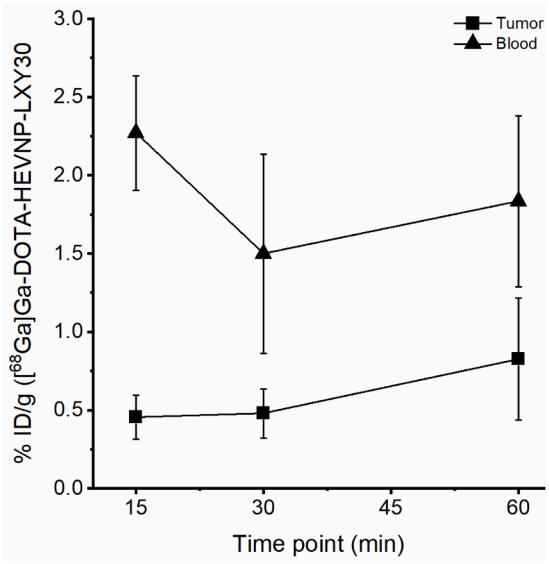

Fig. 5. Comparison of the radioactivity level between the blood and tumor, against time following the *ex vivo* biodistribution of [^{68}Ga]Ga-DOTA-HEVNP-LXY30 in HCT 116 colorectal tumor-bearing female nude NMRI mice. The data denotes the average ± standard deviation (n = 4).

of [^{68}Ga]Ga-DOTA-HEVNP-LXY30 following the *ex vivo* biodistribution in the tumor-bearing nude NMRI mice. The most profound difference was shown in the case of the liver (15% difference on average) and spleen (17% difference on average but with an exception at 15 min where it reached 27%). The highest liver uptake values were due to [^{68}Ga]Ga-DOTA-HEVNP, whereas in the spleen, the [^{68}Ga]Ga-DOTA-HEVNP-LXY30 uptake was the one that gave the highest values. On the other hand, highly similar blood and liver uptake was obtained for the two HEVNP types. In order to increase the tumor uptake of [^{68}Ga]Ga-DOTA-HEVNP-LXY30, the surface of the NPs could be further engineered for example by masking the polysaccharide binding sites responsible for the capsid protein (ORF2)– hepatocyte interaction and therefore aiming at suppressing the liver uptake (Kapur et al., 2012).

Furthermore, autoradiographic analysis of the intratumoral radioactivity distribution was carried out for tumors harvested and cryosectioned at 60 min after the [^{68}Ga]Ga-DOTA-HEVNP-LXY30 or [^{68}Ga]Ga-DOTA-HEVNP administration. In the sections obtained from the tissue at 60 min post-injection, the radioactivity in the tumor was homogeneously distributed. Most of the radiolabeled NPs resided on the tumor surface (Fig.S3 in SI).

Overall, the evaluation of the [^{68}Ga]Ga-DOTA-HEVNP-LXY30 uptake in the HCT 116 colorectal cancer cell line and the tumor was crucial and allowed a deeper understanding of HEVNP biodistribution. Although the targeted uptake *in vivo* was low, this study resulted in the first quantification of the targeting efficacy of the HEVNP system using radiometric methods.

4. Conclusion

HEVNP-LXY30 integrin $\alpha_3\beta_1$-targeted nanoparticles were efficiently radiolabeled with the gallium-68 PET radionuclide. [^{68}Ga]Ga-DOTA-HEVNP-LXY30 remained intact under various conditions *in vitro*. The HCT 116 colorectal cancer cell uptake of the nanosystem was evaluated

and compared to the 4T1 breast cancer cell uptake and the HCT 116 cell uptake of the non-targeted ^{68}Ga-labeled HEVNPs. The [^{68}Ga]Ga-DOTA-HEVNP-LXY30 internalization in the HCT 116 colorectal cells was double the [^{68}Ga]Ga-DOTA-HEVNP internalization, and significantly lower uptake was detected in the case of the 4T1 cells. Although the promising *in vitro* results, the *in vivo* targeting levels of [^{68}Ga]Ga-DOTA-HEVNP-LXY30 toward HCT 116 tumors were low. This observation could be explained by the immediate and high liver uptake of HEVNPs. However, this still is an important observation, and in future studies, the influence on colorectal targeting due to liver uptake could be more carefully examined. This could be done by comparing the results from the current study with the outcome when the HEVNP system is further modified to reduce liver uptake.

All authors contributed to the study conception and design. Material preparation, data collection and analysis were done by EL and contributed by other authors. The first draft of the manuscript was written by EL, and all authors reviewed, commented and edited the manuscript. All authors read and approved the final version of the manuscript. Conceptualization: EL, MS, HC, AA. HEVNP construction and functionalization: CC, EL, HC. Radiochemistry: EL, DL, AA. *In vitro* and *ex vivo*: EL, DL, AS, MS, AA. Resources: HC, AA. Funding: MS, HC, AA. Supervision: HC, AA.

Data availability

Data will be made available on request.

Acknowledgments

This work was financially supported by the Academy of Finland (decision numbers: 298481, 320102, and 318422) and the Alfred Kordelin Foundation, US National Institute of Health (No. TR002866, CA198880, CA225266, EB021230), National Institute Food Agriculture (No. CADMCB-7399-H), and Sigrid Juselius Foundation. The authors would like to thank the Electron Microscopy unit of the University of Helsinki (Institute of Biotechnology) for assistance with the TEM measurements.

Supplementary materials

Supplementary material associated with this article can be found, in the online version, at doi:10.1016/j.ejps.2022.106336.

References

Ahmed, N., Oliva, K., Wang, Y., Quinn, M., Rice, G., 2003. Downregulation of Urokinase plasminogen activator receptor expression inhibits ERK signalling with concomitant suppression of invasiveness due to loss of UPAR–B1 integrin complex in colon cancer cells. Br. J. Cancer 89, 374–384.

Baikoghli, M.A., Chen, C.-C., Nguyen, M., Cheng, R.H., 2018. Enhanced stability of hepatitis E virus nanoparticles via au-nanocluster surface modulation. Nanomed. Nanotechnol. J. 2 (1), 116.

Cao, D., Meng, X.-J., 2012. Molecular biology and replication of hepatitis E virus. Emerg. Microbes Infect. 1 (1), 1–10. https://doi.org/10.1038/emi.2012.7.

Carney, R.P., Hazari, S., Rojalin, T., Knudson, A., Gao, T., Tang, Y., Liu, R., Viitala, T., Yliperttula, M., Lam, K.S., 2017. Targeting tumor-associated exosomes with integrin-binding peptides. Adv. Biosyst. 1 (5), 1600038 https://doi.org/10.1002/adbi.201600038.

Chen, X., Hou, Y., Tohme, M., Park, R., Khankaldyyan, V., Gonzales-Gomez, I., Bading, J. R., Laug, W.E., Conti, P.S., 2004. Pegylated Arg-Gly-Asp Peptide: 64Cu labeling and PET imaging of brain tumor αvβ3-integrin expression. J. Nucl. Med. 45 (10), 1776–1783.

Chen, C.-C., Xing, L., Stark, M., Ou, T., Holla, P., Xiao, K., Kamita, S.G., Hammock, B.D., Lam, K., Cheng, R.H., 2016. Chemically activatable viral capsid functionalized for cancer targeting. Nanomed 11 (4), 377–390. https://doi.org/10.2217/nnm.15.207.

Cheng, R.H.Hepatitis E Nanoparticle, 2018. A capsid-based platform for non-invasive vaccine delivery and imaging-guided cancer treatment. Adv. Res. Gastroenterol. Hepatol. 9 (1) https://doi.org/10.19080/ARGH.2018.09.555752.

Chin, Y.-T., He, Z.-R., Chen, C.-L., Chu, H.-C., Ho, Y., Su, P.-Y., Yang, Y.-C.S.H., Wang, K., Shih, Y.-J., Chen, Y.-R., Pedersen, J.Z., Incerpi, S., Nana, A.W., Tang, H.-Y., Lin, H.-Y., Mousa, S.A., Davis, P.J., Whang-Peng, J., 2019. Tetrac and NDAT induce anti-proliferation via integrin Avβ3 in colorectal cancers with different K-RAS status. Front. Endocrinol. 12 (10), 130. https://doi.org/10.3389/fendo.2019.00130.

Dydensborg, A.B., Teller, I.C., Groulx, J.-F., Basora, N., Paré, F., Herring, E., Gauthier, R., Jean, D., Beaulieu, J.-F., 2009. Integrin A6Bβ4 inhibits colon cancer cell proliferation and C-Myc activity. BMC Cancer 9 (1), 223. https://doi.org/10.1186/1471-2407-9-223.

Ganganboina, A.B., Takemura, K., Zhang, W., Li, T.-C., Park, E.Y., 2021. Cargo encapsulated hepatitis E virus-like particles for anti-HEV antibody detection. Biosens. Bioelectron. 185, 113261 https://doi.org/10.1016/j.bios.2021.113261.

G Kamita, S., A Baikoghli, M., M de la Maza, L., Cheng, R.H., 2020. A noninvasive, orally stable, mucosa-penetrating polyvalent vaccine platform based on hepatitis E virus nanoparticle. In: Nagpal, L., Boldura, M., Baltă, O.-M., C, Enany, S. (Eds.), Synthetic Biology - New Interdisciplinary Science. IntechOpen. https://doi.org/10.5772/intechopen.86830.

Goetz, M., Wang, T.D., 2010. Molecular imaging in gastrointestinal endoscopy. Gastroenterology 138 (3), 828–833. https://doi.org/10.1053/j.gastro.2010.01.009.e1.

He, H., Liu, L., Morin, E.E., Liu, M., Schwendeman, A., 2019. Survey of clinical translation of cancer nanomedicines—lessons learned from successes and failures. Acc. Chem. Res. 52 (9), 2445–2461. https://doi.org/10.1021/acs.accounts.9b00228.

Horibe, S., Tanahashi, T., Kawauchi, S., Murakami, Y., Rikitake, Y., 2018. Mechanism of recipient cell-dependent differences in exosome uptake. BMC Cancer 18 (1), 47. https://doi.org/10.1186/s12885-017-3958-1.

Jariyapong, P., Xing, L., van Houten, N.E., Li, T.-C., Weerachatyanukul, W., Hsieh, B., Moscoso, C.G., Chen, C.-C., Niikura, M., Cheng, R.H., 2013. Chimeric hepatitis E virus-like particle as a carrier for oral-delivery. Vaccine 31 (2), 417–424. https://doi.org/10.1016/j.vaccine.2012.10.073.

Kapur, N., Thakral, D., Durgapal, H., Panda, S.K., 2012. Hepatitis E virus enters liver cells through receptor-dependent clathrin-mediated endocytosis: HEV entry into hepatocytes. J. Viral Hepat. 19 (6), 436–448. https://doi.org/10.1111/j.1365-2893.2011.01559.x.

Kashihara, T., Muguruma, N., Fujimoto, S., Miyamoto, Y., Sato, Y., Takayama, T., 2021. Recent advances in molecular imaging of colorectal tumors. Digestion 102 (1), 57–64. https://doi.org/10.1159/000512168.

Kim, J., Do, E., Moinova, H., Bae, S.M., Kang, J.Y., Hong, S.-M., Fink, S.P., Joo, J., Suh, Y.-A., Jang, S.J., Hwang, S.W., Park, S.H., Yang, D.-H., Ye, B.D., Byeon, J.-S., Choe, J., Yang, S.-K., Markowitz, S.D., Kim, S.-Y., Myung, S.-J., 2017. Molecular imaging of colorectal tumors by targeting colon cancer secreted protein-2 (CCSP-2). Neoplasia N. Y. N 19 (10), 805–816. https://doi.org/10.1016/j.neo.2017.07.003.

Koudelka, K.J., Manchester, M., 2010. Chemically modified viruses: principles and applications. Curr. Opin. Chem. Biol. 14 (6), 810–817. https://doi.org/10.1016/j.cbpa.2010.10.005.

Labianca, R., Beretta, G.D., Kildani, B., Milesi, L., Merlin, F., Mosconi, S., Pessi, M.A., Prochilo, T., Quadri, A., Gatta, G., de Braud, F., Wils, J., 2010. Colon cancer. Crit. Rev. Oncol. Hematol. 74 (2), 106–133. https://doi.org/10.1016/j.critrevonc.2010.01.010.

Lambidis, E, Chen, C-C, Baikoghli, M, Imlimthan, S, Khng, YC, Sarparanta, M, et al., 2022. Development of 68Ga-labeled hepatitis E virus nanoparticles for targeted drug delivery and diagnostics with PET. Mol Pharm. https://doi.org/10.1021/acs.molpharmaceut.2c00359.

Lee, E.B., Kim, J.-H., Hur, W., Choi, J.E., Kim, S.M., Park, D.J., Kang, B.-Y., Lee, G.W., Yoon, S.K., 2019. Liver-specific gene delivery using engineered virus-like particles of hepatitis E virus. Sci. Rep. 9 (1), 1616. https://doi.org/10.1038/s41598-019-38533-7.

Ludvigsen, M., Thorlacius-Ussing, L., Vorum, H., Moyer, M.P., Stender, M.T., Thorlacius-Ussing, O., Honoré, B., 2020. Proteomic characterization of colorectal cancer cells versus normal-derived colon mucosa cells: approaching identification of novel diagnostic protein biomarkers in colorectal cancer. Int. J. Mol. Sci. 21 (10), E3466. https://doi.org/10.3390/ijms21103466.

Maraming, P., Klaynongsruang, S., Boonsiri, P., Peng, S.-F., Daduang, S., Leelayuwat, C., Pientong, C., Chung, J.-G., Daduang, J., 2019. The cationic cell-penetrating KT2 peptide promotes cell membrane defects and apoptosis with autophagy inhibition in human HCT 116 colon cancer cells. J. Cell. Physiol. 234 (12), 22116–22129. https://doi.org/10.1002/jcp.28774.

Pagana, K.D., Pagana, T.J., Pagana, T.N., 2015. Mosby's Diagnostic and Laboratory Test Reference, 12th. Elsevier.

Panda, S.K., Kapur, N., Paliwal, D., Durgapal, H., 2015. Recombinant hepatitis E virus like particles can function as RNA nanocarriers. J. Nanobiotechnology 13 (1), 44. https://doi.org/10.1186/s12951-015-0101-9.

Parkin, D.M., Bray, F., Ferlay, J., Pisani, P., 2005. Global cancer statistics, 2002. CA. Cancer J. Clin. 55 (2), 74–108. https://doi.org/10.3322/canjclin.55.2.74.

Pelillo, C., Bergamo, A., Mollica, H., Bestagno, M., Sava, G., 2015. Colorectal cancer metastases settle in the hepatic microenvironment through A5β1 integrin. J. Cell. Biochem. 116 https://doi.org/10.1002/jcb.25189.

Rohovie, M.J., Nagasawa, M., Swartz, J.R., 2017. Virus-like particles: next-generation nanoparticles for targeted therapeutic delivery: ROHOVIE et Al. Bioeng. Transl. Med. 2 (1), 43–57. https://doi.org/10.1002/btm2.10049.

Senapati, S., Mahanta, A.K., Kumar, S., Maiti, P., 2018. Controlled drug delivery vehicles for cancer treatment and their performance. Signal Transduct. Target. Ther. 3 (1), 1–19. https://doi.org/10.1038/s41392-017-0004-3.

Sloan, E.K., Pouliot, N., Stanley, K.L., Chia, J., Moseley, J.M., Hards, D.K., Anderson, R. L., 2006. Tumor-specific expression of Avβ3 integrin promotes spontaneous metastasis of breast cancer to bone. Breast Cancer Res. 8 (2), R20. https://doi.org/10.1186/bcr1398.

Smith, M.T., Hawes, A.K., Bundy, B.C., 2013. Reengineering viruses and virus-like particles through chemical functionalization strategies. Curr. Opin. Biotechnol. 24 (4), 620–626. https://doi.org/10.1016/j.copbio.2013.01.011.

Takamura, S., Niikura, M., Li, T.-C., Takeda, N., Kusagawa, S., Takebe, Y., Miyamura, T., Yasutomi, Y., 2004. DNA vaccine-encapsulated virus-like particles derived from an orally transmissible virus stimulate mucosal and systemic immune responses by oral administration. Gene Ther. 11 (7), 628–635. https://doi.org/10.1038/sj.gt.3302193.

Wahab, S., Alshahrani, M.Y., Ahmad, M.F., Abbas, H., 2021. Current trends and future perspectives of nanomedicine for the management of colon cancer. Eur. J. Pharmacol. 910, 174464 https://doi.org/10.1016/j.ejphar.2021.174464.

Wang, L., Xia, J., Fan, H., Hou, M., Wang, H., Wang, X., Zhang, K., Cao, L., Liu, X., Ling, J., Yu, H., Wu, X., Sun, J., 2021. A tumor microenvironment responsive nanosystem for chemodynamic/chemical synergistic theranostics of colorectal cancer. Theranostics 11 (18), 8909–8925. https://doi.org/10.7150/thno.61651.

Xiao, W., Li, T., Bononi, F.C., Lac, D., Kekessie, I.A., Liu, Y., Sanchez, E., Mazloom, A., Ma, A., Lin, J., Tran, J., Yang, K., Lam, K.S., Liu, R., 2016. Discovery and characterization of a high-affinity and high-specificity peptide ligand LXY30 for in vivo targeting of A3 integrin-expressing human tumors. EJNMMI Res. 6 (1), 18. https://doi.org/10.1186/s13550-016-0165-z.

Xiao, W., Ma, W., Wei, S., Li, Q., Liu, R., Carney, R.P., Yang, K., Lee, J., Nyugen, A., Yoneda, K.Y., Lam, K.S., Li, T., 2019. High-affinity peptide ligand LXY30 for targeting A3β1 integrin in non-small cell lung cancer. J. Hematol. Oncol. 12 (1), 56. https://doi.org/10.1186/s13045-019-0740-7.

Xie, Y.-H., Chen, Y.-X., Fang, J.-Y., 2020. Comprehensive review of targeted therapy for colorectal cancer. Signal Transduct. Target. Ther. 5 (1), 1–30. https://doi.org/10.1038/s41392-020-0116-z.

Xing, L., Kato, K., Li, T., Takeda, N., Miyamura, T., Hammar, L., Cheng, R.H., 1999. Recombinant hepatitis E capsid protein self-assembles into a dual-domain T = 1 particle presenting native virus epitopes. Virology 265 (1), 35–45. https://doi.org/10.1006/viro.1999.0005.

Zafrullah, M., Khursheed, Z., Yadav, S., Sahgal, D., Jameel, S., Ahmad, F., 2004. Acidic PH enhances structure and structural stability of the capsid protein of hepatitis E virus. Biochem. Biophys. Res. Commun. 313 (1), 67–73. https://doi.org/10.1016/j.bbrc.2003.11.088.

Zheng, Z.-Z., Miao, J., Zhao, M., Tang, M., Yeo, A.E.T., Yu, H., Zhang, J., Xia, N.-S., 2010. Role of heat-shock protein 90 in hepatitis E virus capsid trafficking. J. Gen. Virol. 91 (7), 1728–1736. https://doi.org/10.1099/vir.0.019323-0.